New Limit on the Lepton-Flavor-Violating Decay $\mu^+ \to e^+\gamma$

J. Adam,[1,2] X. Bai,[3] A. M. Baldini,[4a] E. Baracchini,[5] C. Bemporad,[4a,4b] G. Boca,[6a,6b] P. W. Cattaneo,[6a] G. Cavoto,[7] F. Cei,[4a,4b] C. Cerri,[4a] A. de Bari,[6a,6b] M. De Gerone,[8a,8b] T. Doke,[9] S. Dussoni,[8a,8b] J. Egger,[1] K. Fratini,[8a,8b] Y. Fujii,[3] L. Galli,[4a,4b] G. Gallucci,[4a,4b] F. Gatti,[8a,8b] B. Golden,[5] M. Grassi,[4a] D. N. Grigoriev,[10] T. Haruyama,[11] M. Hildebrandt,[1] Y. Hisamatsu,[3] F. Ignatov,[10] T. Iwamoto,[3] P.-R. Kettle,[1] B. I. Khazin,[10] O. Kiselev,[1] A. Korenchenko,[12] N. Kravchuk,[12] A. Maki,[11] S. Mihara,[11] W. Molzon,[5] T. Mori,[3] D. Mzavia,[12,*] H. Natori,[3,1] D. Nicolò,[4a,4b] H. Nishiguchi,[11] Y. Nishimura,[3,†] W. Ootani,[3] M. Panareo,[13a,13b] A. Papa,[1] R. Pazzi,[4a,4b,*] G. Piredda,[7] A. Popov,[10] F. Renga,[7,1] S. Ritt,[1] M. Rossella,[6a] R. Sawada,[3] F. Sergiampietri,[4a] G. Signorelli,[4a] S. Suzuki,[9] F. Tenchini,[4a,4b] C. Topchyan,[5] Y. Uchiyama,[3,1] R. Valle,[8a,8b,‡] C. Voena,[7] F. Xiao,[5] S. Yamada,[11] A. Yamamoto,[11] S. Yamashita,[3] Yu. V. Yudin,[10] and D. Zanello[7]

(MEG Collaboration)

[1]*Paul Scherrer Institut PSI, CH-5232 Villigen, Switzerland*
[2]*Swiss Federal Institute of Technology ETH, CH-8093 Zürich, Switzerland*
[3]*ICEPP, University of Tokyo, 7-3-1 Hongo, Bunkyo-ku, Tokyo 113-0033, Japan*
[4a]*INFN Sezione di Pisa, Largo B. Pontecorvo 3, 56127 Pisa, Italy*
[4b]*Dipartimento di Fisica dell'Università, Largo B. Pontecorvo 3, 56127 Pisa, Italy*
[5]*University of California, Irvine, California 92697, USA*
[6a]*INFN Sezione di Pavia, Via Bassi 6, 27100 Pavia, Italy*
[6b]*Dipartimento di Fisica Nucleare e Teorica dell'Università, Via Bassi 6, 27100 Pavia, Italy*
[7]*INFN Sezione di Roma, Piazzale A. Moro, 00185 Roma, Italy*
[8a]*INFN Sezione di Genovaa, Via Dodecaneso 33, 16146 Genova, Italy*
[8b]*Dipartimento di Fisicab dell'Università, Via Dodecaneso 33, 16146 Genova, Italy*
[9]*Research Institute for Science and Engineering, Waseda University, 3-4-1 Okubo, Shinjuku-ku, Tokyo 169-8555, Japan*
[10]*Budker Institute of Nuclear Physics, 630090 Novosibirsk, Russia*
[11]*KEK, High Energy Accelerator Research Organization, 1-1 Oho, Tsukuba, Ibaraki 305-0801, Japan*
[12]*Joint Institute for Nuclear Research, 141980, Dubna, Russia*
[13a]*INFN Sezione di Leccea, Via per Arnesano, 73100 Lecce, Italy*
[13b]*Dipartimento di Fisicab dell'Università, Via per Arnesano, 73100 Lecce, Italy*
(Received 31 July 2011; published 17 October 2011)

We present a new result based on an analysis of the data collected by the MEG detector at the Paul Scherrer Institut in 2009 and 2010, in search of the lepton-flavor-violating decay $\mu^+ \to e^+\gamma$. The likelihood analysis of the combined data sample, which corresponds to a total of 1.8×10^{14} muon decays, gives a 90% C.L. upper limit of 2.4×10^{-12} on the branching ratio of the $\mu^+ \to e^+\gamma$ decay, constituting the most stringent limit on the existence of this decay to date.

DOI: 10.1103/PhysRevLett.107.171801 PACS numbers: 13.35.Bv, 11.30.Hv, 12.10.Dm, 12.60.Jv

The lepton-flavor-violating decay $\mu \to e\gamma$ is forbidden within the standard model (SM) of elementary particles. Even with the introduction of neutrino masses and mixing SM predicts an immeasurably small branching ratio ($\mathcal{B} \lesssim 10^{-51}$) for this decay. Conversely, new physics scenarios beyond SM, such as supersymmetric grand unified theories or theories with extra dimensions, predict branching ratios in the 10^{-12} to 10^{-14} range [1–3]. This is close to the present limit set by the MEGA experiment [4], $\mathcal{B} \leq 1.2 \times 10^{-11}$, which places one of the most stringent constraints on the formulation of such theories. Observation of $\mu \to e\gamma$ therefore would be an unambiguous signature of new physics, while improvements on the existing limit would stringently constrain many of the new physics scenarios beyond the SM.

The MEG experiment [5,6] covers a 10% solid angle, centered around a thin muon stopping target (205 μm-thick polyethylene) and is composed of a positron spectrometer and a photon detector in search of back-to-back, monoenergetic, time coincident photons and positrons from the two-body $\mu^+ \to e^+\gamma$ decays. The positron spectrometer consists of a set of drift chambers (DC) [7] and scintillation timing counters (TC) [8] located inside a superconducting solenoid with a gradient field [9] along the beam axis, ranging from 1.27 T at the center to 0.49 T at either end. The photon detector [10], located outside of the solenoid, is a homogeneous volume (900 l) of liquid xenon (LXe) viewed by 846 UV-sensitive photomultiplier tubes (PMTs) submerged in the liquid. The spectrometer measures the positron momentum vector and timing, while the

LXe detector is used to reconstruct the γ-ray energy as well as the position and time of its first interaction in LXe. All the signals are individually digitized by in-house designed waveform digitizers based on the multi-GHz domino ring sampler chip (DRS) [11]. The Paul Scherrer Institut (PSI) πE5 beam line is used to stop 3×10^7 positive muons per second in the target. The residual polarization of the decaying muons along the beam axis was measured to be $\langle P \rangle = -0.89 \pm 0.04$. The background to $\mu^+ \to e^+\gamma$ decay comes either from radiative muon decays (RMD) $\mu^+ \to e^+\nu\bar{\nu}\gamma$ in which the neutrinos carry away little energy or from an accidental coincidence of an energetic positron from a normal Michel decay with a γ ray coming from RMD, bremsstrahlung, or positron annihilation in flight. The accidental coincidences are the dominant background in this experiment.

The MEG detector response, resolutions, and stability are constantly monitored and calibrated. The PMTs of the LXe detector are calibrated daily by light-emitting diodes and α sources immersed in the liquid [12]. The energy scale and resolutions of the LXe detector are measured over the energy range of 4.43–129.4 MeV using γ rays from a radioactive Am-Be source, (p, γ) reaction using a dedicated Cockcroft-Walton accelerator [13], and $\pi^- p$ charge exchange (CEX) and radiative capture reactions. A 9 MeV γ line from the capture in nickel of neutrons from a pulsed and triggerable deuteron-deuteron neutron generator allows one to check the stability of the LXe detector even during data taking. The relative time between the TC and LXe detector is monitored using RMD and 2γ events from ${}^{11}_{5}\mathrm{B}(p, 2\gamma){}^{12}_{6}\mathrm{C}$ reactions.

The $\mu^+ \to e^+\gamma$ trigger requires the presence of a high energy γ ray in the LXe detector and a hit on the timing counters within a 20 ns window together with an approximate back-to-back topology. Prescaled monitoring and calibration triggers are also recorded. A more detailed description of the MEG detector can be found in Ref. [6].

The results presented in this Letter are based on data collected in 2009 and 2010 (for a total of 1.8×10^{14} μ^+ decays in the target); the 2010 statistics are about twice that of 2009. All subdetectors were running stably during these periods. The 2008 data [6] are not used in this analysis because of their limited statistics and detector performance. In 2010 a DRS upgrade resulted in an improvement in the time resolution while an increase in noise in the DC, due to a deterioration of the high-voltage power supplies, caused slightly worse positron tracking resolutions.

We adopted a likelihood analysis method combined with a blind procedure on examining the data: events close to the signal region were kept hidden (blind region) until all the analysis procedures had been completely defined. The probability density functions (PDFs) needed for the likelihood analysis were constructed using the events outside of the blind region (sidebands).

Several improvements to the analysis have been introduced since the presentation of the preliminary result based on the 2009 data [14] and also implemented in the current 2009, as well as in our 2010, analyses. These improvements include a new alignment technique for the DC system, an improved experimental evaluation of the spectrometer performances, a better understanding of the gradient magnetic field, improvement in the relative alignment of the photon detector and the positron spectrometer by means of cosmic ray muons, adoption of a more commonly used statistical method (profile likelihood), and a constraint on the background rates in the likelihood analysis from the data in the sidebands.

The kinematic variables used to identify the $\mu^+ \to e^+\gamma$ decays are the γ-ray and e^+ energies (E_γ, E_e), their relative directions ($\theta_{e\gamma}$, $\phi_{e\gamma}$) [15], and emission time ($t_{e\gamma}$). The off-line event selection requires at least one e^+ track reconstructed in the spectrometer and pointing to the target, with minimal quality cuts applied. The blind region is defined by $48 < E_\gamma < 58$ MeV and $|t_{e\gamma}| < 1$ ns.

The positron track reconstruction in the spectrometer is based on a Kalman filter technique [16]. Effects of multiple scattering and energy loss in the detector materials in the presence of the nonuniform magnetic field are taken into account. Internal alignment of the DC is obtained by tracking cosmic ray muons without a magnetic field and by minimizing the measured residuals in a manner independent of the initially assumed alignment [17]. The absolute position of the DC system is based on an optical survey.

The magnetic field of the spectrometer was measured at the beginning of the experiment and only its major component along the beam axis is used in the analysis to avoid possible misalignment errors from the Hall probes; the other minor components are deduced from the derivatives of the measured primary component using Maxwell equations together with boundary conditions at a symmetry plane at the magnet center where the minor components are nearly zero. This magnetic field map agrees to within 0.2% with the field computed for the geometry and currents of the spectrometer coils.

The resolutions of the positron track direction are estimated by exploiting tracks with two full turns in the DC. Each turn is treated as an independent track and the resolutions are extracted from the difference between the two reconstructed sections. The energy resolution is evaluated by fitting the kinematic edge of the Michel decays and is well described by a sum of three Gaussians with resolutions of 0.31, 1.1, and 2.0 MeV for the core (80%) and the two tail (13% and 7%) components, respectively, for 2009 and 0.32, 1.0, and 2.0 MeV for the core (79%) and the two tail (14% and 7%) components, respectively, for 2010.

The decay vertex coordinates and the positron direction at the vertex are determined by extrapolating the reconstructed track back to the target. The γ-ray direction is defined by the line connecting the decay vertex to the γ-ray conversion point measured by the LXe detector.

A geometrical correlation exists between errors on ϕ_e at the vertex position and E_e, which is measured by using the two-turn method and is perfectly reproduced by the Monte Carlo (MC) simulation. The ϕ_e resolution has a ϕ_e dependence due to the correlation and has a minimum at $\phi_e = 0$, where it is measured to be $\sigma_{\phi_e} = 6.7$ (7.2) mrad for 2009 (2010) data. (From here on we will quote in parentheses the value in the 2010 data when different from that in 2009.) The θ_e resolution is measured by the two-turn method to be $\sigma_{\theta_e} = 9.4$ (11.0) mrad. The resolution on the decay vertex coordinates is also determined by the two-turn method; along the beam axis it is described by a Gaussian with $\sigma_z = 1.5$ (2.0) mm while in the vertical direction it is described by the sum of two Gaussians with $\sigma_y = 1.1$ mm for the core [87% (85%)] and $\sigma_y = 5.3$ (4.8) mm for the tail.

The determination of the photon energy E_γ in the LXe detector is based on the sum of the number of scintillation photons detected by the PMTs; correction factors take into account the different PMT geometrical acceptances. Because of its geometry the detector response is not totally uniform over the photon entrance window; this is corrected for by using γ lines from Cockcroft-Walton and CEX reactions. The absolute energy scale and resolution at the signal energy $E_\gamma = 52.8$ MeV are determined by the CEX measurement; the resolution σ_R, extracted from a Gaussian fit to the high energy side of the spectrum, depends also on the depth (w) of the γ-ray conversion point from the photon entrance surface of the LXe detector: $\sigma_R = 1.9\%$ ($w > 2$ cm) and 2.4% ($w < 2$ cm). The 3D map of the measured resolutions is incorporated into the PDFs for the likelihood analysis.

The photon energy scale and the resolutions are cross-checked by fitting the background spectra measured in the sidebands with the theoretical RMD spectrum folded with the detector resolutions; the resolutions during the run are well represented by the CEX evaluations, and the systematic uncertainty of the E_γ scale is estimated to be $\simeq 0.3\%$. Since MEG operates at a high beam intensity, it is important to recognize and unfold pile-up photons. For each event the spatial and temporal distributions of the PMT charge are studied to identify photon pile up in the LXe detector; in the case of positive identification, corrections to the PMT charges are applied. Cosmic ray events are rejected using their characteristic PMT charge distribution.

The position of the first interaction of the γ ray in the LXe detector is derived from the light distribution measured by the PMTs close to the region of the energy deposition by fitting the distribution with the expectation. The position resolution in the plane of the photon entrance window is measured to be 5 mm in a dedicated CEX run with a lead slit collimator placed in front of the LXe detector, while the resolution along the depth w of 6 mm and the position dependence of the resolutions are evaluated by MC simulation.

The resolutions on the relative directions ($\theta_{e\gamma}$, $\phi_{e\gamma}$) are derived by combining the relevant resolutions of positrons and photons discussed above; the results are 14.5 (17.1) mrad for $\theta_{e\gamma}$ and 13.1 (14.0) mrad for $\phi_{e\gamma}$. The relative time $t_{e\gamma}$ is derived from the two time measurements by the LXe detector and the TC, after correcting for the length of the particle flight path. The associated resolutions at the signal energy 146 (122) ps are evaluated from the RMD peak observed in the E_γ sideband; a small correction takes into account the E_γ dependence measured in the CEX calibration runs. The position of the RMD peak corresponding to $t_{e\gamma} = 0$ was monitored constantly during the physics data-taking period and found to be stable to within 15 ps.

A likelihood analysis is carried out for events in a portion of the blind region (analysis region) defined by $48 < E_\gamma < 58$ MeV, $50 < E_e < 56$ MeV, $|t_{e\gamma}| < 0.7$ ns, $|\theta_{e\gamma}| < 50$ mrad, and $|\phi_{e\gamma}| < 50$ mrad. These intervals in the analysis variables are between 5σ and 20σ wide to fully contain the signal events and also retain some background events. The best estimates of the numbers of signal, RMD, and accidental background (BG) events in the analysis region are obtained by maximizing the following likelihood function:

$$\mathcal{L}(N_{\rm sig}, N_{\rm RMD}, N_{\rm BG}) = \frac{e^{-N}}{N_{\rm obs}!} e^{-[(N_{\rm RMD}-\langle N_{\rm RMD}\rangle)^2/2\sigma^2_{\rm RMD}]} \times e^{-[(N_{\rm BG}-\langle N_{\rm BG}\rangle)^2/2\sigma^2_{\rm BG}]} \prod_{i=1}^{N_{\rm obs}} [N_{\rm sig} S(\vec{x}_i) + N_{\rm RMD} R(\vec{x}_i) + N_{\rm BG} B(\vec{x}_i)],$$

where $\vec{x}_i = \{E_\gamma, E_e, t_{e\gamma}, \theta_{e\gamma}, \phi_{e\gamma}\}$ is the vector of observables for the ith event, $N_{\rm sig}$, $N_{\rm RMD}$, and $N_{\rm BG}$ are the expected numbers of signal, RMD, and BG events, while S, R, and B are their corresponding PDFs. $N = N_{\rm sig} + N_{\rm RMD} + N_{\rm BG}$ and $N_{\rm obs}$ [= 311 (645)] is the observed total number of events in the analysis window. $\langle N_{\rm RMD}\rangle$ [= 27.2 (52.2)], and $\langle N_{\rm BG}\rangle$ [= 270.9 (610.8)] are the numbers of RMD and BG events extrapolated from the sidebands together with their uncertainties $\sigma_{\rm RMD}$ [= 2.8 (6.0)] and $\sigma_{\rm BG}$ [= 8.3 (12.6)], respectively.

The signal PDF $S(\vec{x}_i)$ is the product of the PDFs for E_e, $\theta_{e\gamma}$, $\phi_{e\gamma}$, and $t_{e\gamma}$, which are correlated variables, as explained above, and the E_γ PDF. The PDFs properly incorporate the measured resolutions and correlations among E_e, $\theta_{e\gamma}$, $\phi_{e\gamma}$, and $t_{e\gamma}$ on an event-by-event basis. The RMD PDF $R(\vec{x}_i)$ is the product of the same $t_{e\gamma}$ PDF as that of the signal and the PDF of the other four correlated observables, which is formed by folding the theoretical spectrum with the detector response functions. The BG PDF $B(\vec{x}_i)$ is the product of the five PDFs, each of which is defined by the single background spectrum, precisely measured in the sidebands. The dependence of the resolutions on the

position of the γ-ray interaction point and on the positron tracking quality is taken into account in the PDFs.

A frequentist approach with a profile likelihood-ratio ordering [18,19] is used to compute the confidence intervals on $N_{\rm sig}$:

$$\lambda_p(N_{\rm sig}) = \frac{\mathcal{L}(N_{\rm sig}, \hat{\hat{N}}_{\rm RMD}(N_{\rm sig}), \hat{\hat{N}}_{\rm BG}(N_{\rm sig}))}{\mathcal{L}(\hat{N}_{\rm sig}, \hat{N}_{\rm RMD}, \hat{N}_{\rm BG})},$$

where the hat and double hat denote the best estimates maximizing the likelihood for floating and fixed $N_{\rm sig}$, respectively. Other, independent analysis schemes based on averaged PDFs without event-by-event information or Bayesian approach were also used and found to be compatible with the analysis presented here to within 10%–20% difference in the obtained branching ratio upper limits.

In order to convert $N_{\rm sig}$ into a branching ratio value the normalization relative to the Michel decay is computed [6] by counting the number of Michel positrons passing the same analysis cuts. This is accomplished by means of a prescaled Michel positron trigger enabled during the physics data taking. A correction to the prescaling factor due to positron pileup in the TC is taken into account. Another method for computing the normalization uses RMD events in the E_γ sideband and the theoretical branching ratio of the RMD. The normalizations calculated by these two independent methods are in good agreement and are combined to give the normalization factor with a 7% uncertainty.

The sensitivity of the experiment with a null signal hypothesis is evaluated by taking the median of the distribution of the upper limit on the branching ratio obtained over an ensemble of toy MC experiments. The rates of RMD and BG events, as measured in the sidebands, are assumed in the simulated experiments. The branching ratio sensitivity at 90% C.L. is found to be 3.3×10^{-12} (2.2×10^{-12}) for the 2009 (2010) data sample and 1.6×10^{-12} when 2009 and 2010 are combined. These sensitivities are consistent with the upper limits obtained by the likelihood analyses in several comparable analysis regions of the $t_{e\gamma}$ sidebands.

After calibrations, optimization of the analysis algorithms, and background studies in the sidebands are completed, the likelihood analysis in the analysis region is performed. In Fig. 1 we present the distributions for the 2009 and 2010 data samples, respectively, showing the events seen in the analysis region projected in the E_γ vs E_e and $t_{e\gamma}$ vs $\cos\Theta_{e\gamma}$ planes, $\Theta_{e\gamma}$ being the opening angle between the γ ray and the positron. In Figs. 1(a) and 1(c) selections in $t_{e\gamma}$ and $\cos\Theta_{e\gamma}$, each of which is 90% efficient on the signal, are applied ($|t_{e\gamma}| < 0.28$ ns and $\cos\Theta_{e\gamma} < -0.9996$); in Figs. 1(b) and 1(d) a selection in E_e which is 90% efficient on the signal and a selection in E_γ which is 73% efficient on the signal inside the analysis window are applied ($52.3 < E_e < 55$ MeV and $51 < E_\gamma < 55$ MeV). The contours of the signal PDF are also drawn and a few events with the highest signal likelihood are numbered in a decreasing order of relative signal likelihood, $S/(f_R R + f_B B)$, $f_R = 0.1$ and $f_B = 0.9$ being the fractions of the RMD and the BG measured in the sidebands, respectively. High signal likelihood events were thoroughly checked and found to be randomly distributed in time and detector acceptance.

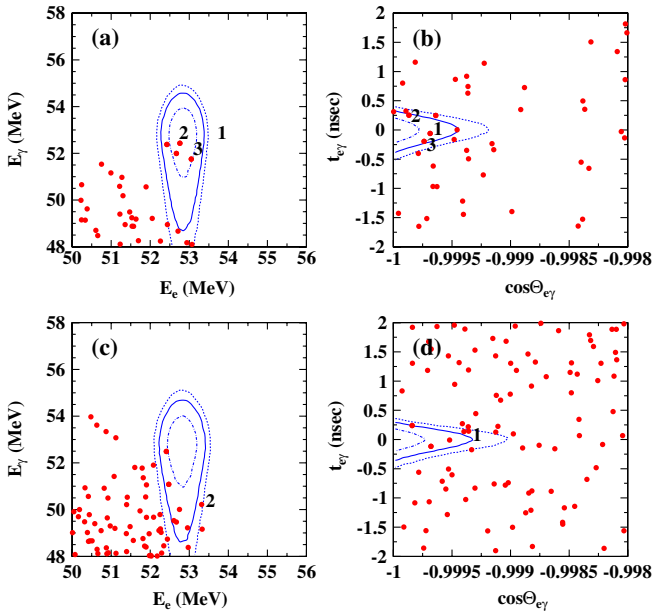

FIG. 1 (color online). Event distributions in the analysis region of (a) E_γ vs E_e and (b) $t_{e\gamma}$ vs $\cos\Theta_{e\gamma}$ for 2009 data and of (c) E_γ vs E_e and (d) $t_{e\gamma}$ vs $\cos\Theta_{e\gamma}$ for 2010 data. The contours of the PDFs (1σ, 1.64σ, and 2σ) are shown, and a few events with the highest signal likelihood are numbered for each year. [The two highest signal likelihood events in 2010 data appear only in (c) or (d).]

The observed profile likelihood ratios as a function of the branching ratio for 2009, 2010, and the combined data sample are shown in Fig. 2 [20]. The analysis of the full data sample gives a 90% C.L. upper limit of 2.4×10^{-12}, which constitutes the most stringent limit on the existence of the

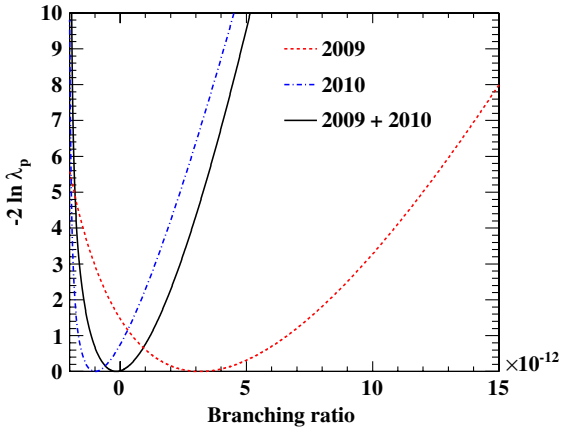

FIG. 2 (color online). Profile likelihood ratios as a function of the $\mu^+ \to e^+\gamma$ branching ratio for 2009, 2010, and the combined 2009 and 2010 data sample.

TABLE I. Best fit ($\mathcal{B}_{\mathrm{fit}}$), lower limits (LL), and upper limits (UL) at the 90% C.L. of the branching ratio for the 2009, 2010, and combined 2009 and 2010 data sets.

Data set	$\mathcal{B}_{\mathrm{fit}}$	LL	UL
2009	3.2×10^{-12}	1.7×10^{-13}	9.6×10^{-12}
2010	-9.9×10^{-13}	$\cdots$	1.7×10^{-12}
2009 and 2010	-1.5×10^{-13}	$\cdots$	2.4×10^{-12}

$\mu^+ \to e^+\gamma$ decay, superseding the previous limit by a factor of 5. The 90% C.L. intervals as well as the best estimate of the branching ratio for 2009 and 2010 data separately are also given in Table I. The 2009 data set, which gives a positive best estimate for the branching ratio, is consistent with the hypothesis $\mathcal{B} = 0$ with an 8% probability.

The systematic uncertainties for the parameters of the PDFs and the normalization factor are taken into account in the calculation of the confidence intervals by fluctuating the PDFs according to the uncertainties. The largest contributions to the systematic uncertainty, which amount to a shift of about 2% in total in the branching ratio upper limit, come from the uncertainties of the offsets of the relative angles, the correlations in the positron observables, and the normalization.

The MEG experiment continues data taking and is expected to explore the $\mu^+ \to e^+\gamma$ decay down to a branching ratio sensitivity of a few times 10^{-13} in the next few years.

*Deceased.

†Present address: Kamioka Observatory, ICRR, University of Tokyo 456 Higashi-Mozumi, Kamioka-cho, Hida-city, Gifu 506-1205, Japan.

‡Present address: Lames Holding S.r.l., 16043 Chiavari, Italy.

[1] R. Barbieri, L. Hall, and A. Strumia, Nucl. Phys. **B445**, 219 (1995).

[2] J. Hisano, D. Nomura, and T. Yanagida, Phys. Lett. B **437**, 351 (1998).

[3] M. Raidal *et al.*, Eur. Phys. J. C **57**, 13 (2008).

[4] M. L. Brooks *et al.* (MEGA Collaboration), Phys. Rev. Lett. **83**, 1521 (1999).

[5] A. Baldini, T. Mori *et al.*, "The MEG experiment: search for the $\mu \to e\gamma$ decay at PSI," http://meg.web.psi.ch/docs/prop_infn/nproposal.pdf.

[6] J. Adam *et al.* (MEG Collaboration), Nucl. Phys. **B834**, 1 (2010).

[7] M. Hildebrandt *et al.* (MEG Collaboration), Nucl. Instrum. Methods Phys. Res., Sect. A **623**, 111 (2010).

[8] M. De Gerone *et al.*, Nucl. Instrum. Methods Phys. Res., Sect. A **638**, 41 (2011).

[9] W. Ootani *et al.*, IEEE Trans. Appl. Supercond. **14**, 568 (2004).

[10] S. Mihara *et al.* (MEG Collaboration), J. Phys. Conf. Ser. **308**, 012009 (2011).

[11] S. Ritt *et al.*, Nucl. Instrum. Methods Phys. Res., Sect. A **623**, 486 (2010).

[12] A. Baldini *et al.*, Nucl. Instrum. Methods Phys. Res., Sect. A **565**, 589 (2006).

[13] J. Adam *et al.* (MEG Collaboration), Nucl. Instrum. Methods Phys. Res., Sect. A **641**, 19 (2011).

[14] A. M. Baldini (MEG Collaboration), Proc. Sci., ICHEP2010 (2010) 528; R. Sawada (MEG Collaboration), Proc. Sci., ICHEP2010 (2010) 263.

[15] $\theta_{e\gamma} = (\pi - \theta_e) - \theta_\gamma$ and $\phi_{e\gamma} = (\pi + \phi_e) - \phi_\gamma$, θ and ϕ being the polar angle and the azimuthal angle, respectively, taking the z axis as the beam axis.

[16] R. Frühwirt *et al.*, *Data Analysis Techniques for High Energy Physics* (Cambridge University Press, Cambridge, England, 2000), 2nd ed.

[17] CMS Collaboration, JINST **5**, T03009 (2010).

[18] K. Nakamura *et al.* (Particle Data Group), J. Phys. G **37**, 075021 (2010).

[19] G. J. Feldman and R. D. Cousins, Phys. Rev. D **57**, 3873 (1998).

[20] These curves are not directly used to derive the upper limits which are obtained in a full frequentist approach as described above.